Disruption of human brain connectivity networks in patients with cervical spondylotic myelopathy

Yuan Cao[1,2,3#], Yaru Zhan[1,4#], Miao Du[5], Guoshu Zhao[1,4], Zhili Liu[6], Fuqing Zhou[1,4], Laichang He[1,4]

[1]Department of Radiology, the First Affiliated Hospital of Nanchang University, Nanchang, China; [2]Department of Nuclear Medicine, West China Hospital of Sichuan University, Chengdu, China; [3]Huaxi MR Research Center, Department of Radiology, West China Hospital of Sichuan University, Chengdu, China; [4]Neuroimaging Lab, Jiangxi Province Medical Imaging Research Institute, Nanchang, China; [5]College of Electrical Engineering of Sichuan University, Chengdu, China; [6]Department of Orthopedic Surgery, the First Affiliated Hospital of Nanchang University, Nanchang, China

[#]These authors contributed equally to this work.

Correspondence to: Dr. Laichang He, MD; Dr. Fuqing Zhou, PhD, MD. Department of Radiology, the First Affiliated Hospital of Nanchang University, 17 Yong Wai Zheng Street, Nanchang 330006, China. Email: laichang_he@163.com; fq.chou@yahoo.com.

Background: Brain functional plasticity and reorganization in patients with cervical spondylotic myelopathy (CSM) is increasingly being explored and validated. However, specific topological alterations in functional networks and their role in CSM brain functional reorganization remain unclear. This study investigates the topological architecture of intrinsic brain functional networks in CSM patients using graph theory.

Methods: Functional MRI was conducted on 67 CSM patients and 60 healthy controls (HCs). The topological organization of the whole-brain functional network was then calculated using theoretical graph analysis. The difference in categorical variables between groups was compared using a chi-squared test, while that between continuous variables was evaluated using a two-sample t-test. Nonparametric permutation tests were used to compare network measures between the two groups.

Results: Small-world architecture in functional brain networks were identified in both CSM patients and HCs. Compared with HCs, CSM patients showed a decreased area under the curve (AUC) of the characteristic path length (FDR q=0.040), clustering coefficient (FDR q=0.037), and normalized characteristic path length (FDR q=0.038) of the network. In contrast, there was an increased AUC of normalized clustering coefficient (FDR q=0.014), small-worldness (FDR q=0.009), and global network efficiency (FDR q=0.027) of the network. In local brain regions, nodal topological properties revealed group differences which were predominantly in the default-mode network (DMN), left postcentral gyrus, bilateral putamen, lingual gyrus, and posterior cingulate gyrus.

Conclusions: This study reported altered functional topological organization in CSM patients. Decreased nodal centralities in the visual cortex and sensory-motor regions may indicate sensory-motor dysfunction and blurred vision. Furthermore, increased nodal centralities in the cerebellum may be compensatory for sensory-motor dysfunction in CSM, while the increased DMN may indicate increased psychological processing in CSM patients.

Keywords: Cervical spondylotic myelopathy; graph theory analysis; functional reorganization; small-world network; brain functional network

Introduction

Cervical spondylotic myelopathy (CSM) is an incomplete spinal cord injury characterized by pain and stiffness in the neck and motor and sensory dysfunction (1,2). The prevalence of CSM in North America is about 605 per million population and shows increasing incidence with age, especially in those aged 50 years and above, although recently there has been an increase in CSM incidence in young people (3,4). Although current evidence indicates improved neurological function after surgery, symptom relief is often dismal or worse in some patients (5,6).

Neurological function recovery in CSM depends on spinal cord compression and injury and cerebral functional reorganization or plasticity (7). This means some brain regions that are not primarily involved in a particular task are called to compensate for this function (8). This cortical plasticity could also present in response to spinal cord injury (9). Sabbah *et al.* found that with some cortical reorganization, the cortical network of the lower extremity can be activated by the attempt of movement or the mental arousal of movement even several years after injury (10). This cortico-spinal neuroplasticity is an adaptive remodeling response to preserve neurological function during spinal cord injury and has been observed in CSM patients (11). Our previous study investigated potential differences in sensorimotor networks' connectedness using functional connectivity strength and indicated the presence of an initial intrinsic functional plasticity in CSM patients (12). Unraveling brain remodeling's complex mechanisms is a critical first step in exploring the cause of different prognostic outcomes in CSM patients.

Noninvasive resting-state functional MRI (rsfMRI) has recently emerged as a powerful imaging modality for studying CSM and spinal cord injuries, further examining brain remodeling, and is particularly useful in functional and structural alterations in the sensory-motor or visual regions. Previously, we measured the activity of amplitude of low-frequency fluctuations (ALFF) within sensory-motor networks in CSM and its association with impaired spinal segments and found that increased ALFF values in the right precentral gyrus and right postcentral gyrus were associated with decreased fractional anisotropy values at the C2 level (13). We then performed a longitudinal study to investigate the regional homogeneity (ReHo) value of CSM patients before and after decompression surgery (14). The results showed that ReHo was decreased in the left primary sensory cortex and primary motor cortex but increased

in the right superior parietal lobule (SPL) and that decompression surgery reversed these changes. The ALFF and ReHo values deficits in the default-mode network (DMN), visual cortex, and motor-related cerebellum area in CSM patients have also been investigated (15). Moreover, a recent neuroimaging study combined intrinsic neuronal functional activity parameters with functional connectivity to further demonstrate innate cortical plasticity in CSM patients (16). These studies provide complementary evidence of cortical functional reorganization in CSM.

Graph theory has been widely used to characterize local and distributed interactions in the brain and provides advanced mathematical tools to show altered topological characteristics in functional brain networks (17). The human brain works in an efficiently small-world model under a complex brain network (18). In graph theory analysis, network efficiency and "small-world" parameters play key roles in showing the organization of the global brain network, which could reflect brain functional integration and separation and the brain's ability to induce defenses in response to the attack. Graph theory has been used to study epilepsy, Alzheimer's disease (AD), major depressive disorder (MDD), primary angle-closure glaucoma, and spinal cord injury (SCI) (19-23). Min *et al.* explored the functional connectivity change of SCI patients by using a graph theory approach, and while no statistically significant difference of clustering coefficient (Cp), global efficiency, or small-worldness was found in SCI patients compared with controls, a higher normalized characteristic path length (λ) was found in SCI patients (19). However, the CSM was a special incomplete SCI, and whether the CSM patients had similar topological properties to those patients with SCI is worth exploring. Previous neuroimaging CSM studies have found a correlation between disease symptoms and functional connectivity in specific resting-state brain regions or networks and indicated the human brain connectome as an underlying biomarker of CSM (16,24). A recent study based on topological characteristics of the structural network in CSM patients found a lower Cp and shorter characteristic path length (Lp) in the brain structural covariance network (25). More specifically, that study indicated a shifting brain structural network trended towards random brain networks and found increased betweenness in sensorimotor-related brain areas, which may support the cortex reorganization theory involved in the recovery of sensory-motor function in CSM patients. Despite this, none of these studies have explored the topological characteristics of the functional network in CSM, and until now, the global

3420

Cao et al. Graph theory analysis of CSM

and regional topological properties of CSM remain largely unknown. However, topological properties such as Cp, Lp, and network efficiency could concisely quantify the complex system of the human brain and help assess how the brain works as a system and evaluate its work efficiency (26). Specifically, a better understanding of altered topological properties of CSM-related brain networks may unravel the underlying mechanism of cortical functional reorganization, shedding light on the different prognoses of CSM patients.

This study aimed to determine the topological architecture of intrinsic brain functional networks in CSM patients using theoretical graph analysis. The link between the topological organization of the functional brain network and patients' clinical condition was evaluated. We hypothesized that global and regional topological properties would be atypical in CSM patients and that identified network alterations would be related to sensory-motor deficits that may further explain cortical functional reorganization in CSM.

Methods

The Institutional Review Board of the First Affiliated Hospital of Nanchang University approved recruitment and data collection procedures. The study was conducted following ethical principles for medical research involving human subjects as stipulated in the World Medical Association's Declaration of Helsinki. Written informed consent was obtained from each subject before the study.

Participants

A total of 70 CSM patients and 66 healthy controls (HCs), all Han Chinese, were initially selected for this study. Data from three patients and six controls were excluded based on head motion greater than 3 mm translation or 3 degrees in any direction during the fMRI scan. A total of 127 participants were finally recruited between May 2014 and May 2019, comprising of 67 CSM patients (35 males and 32 females; mean age 47.52±7.36 years; range 30 to 62 years) and 60 HCs of level-matched age, sex, and education (32 males and 28 females; mean age 45.51±10.64 years; range 25 to 64 years).

Two radiologists independently examined the radiological features of each patient. Thereafter, a diagnosis of CSM was determined by a clinician and the two radiologists (LCH, FQZ, ZLL). Patients were included in the study if they: (I) had clear evidence of cord compression on cervical spine MRI, including cervical spondylosis, herniated discs or ligamentum flavum hypertrophy, and demyelination with hyper-intensity of the cord on T2-weighted images (T2WI); (II) had a primary CSM diagnosis, were not taking medication and had not undergone previous decompression surgery; (III) were aged between 18 and 65 years; (IV) were right-handed, and (V) voluntarily enrolled in the study. The exclusion criteria included: (I) a history of psychiatric disorders; (II) trauma or infection related to cord compression; and (III) pre-existing spinal or brain neurological disorders such as multiple sclerosis.

MRI data acquisition

All MRI scans were performed on a SIEMENS Trio 3.0 Tesla MRI scanner with an 8-channel head coil and sagittal and axial conventional T1-weighted, T2-weighted, and T2-FLAIR (fluid-attenuated inversion recovery) images of the brain and cervical spinal cord were obtained. During the brain rs-fMRI scan, all subjects were instructed to stay awake, keep still with their eyes closed, and not think of anything in particular. An echo-planar imaging (EPI) sequence was used with the following parameters: repetition time/echo time (TR/TE) =2,000/30 ms; field of view (FOV) =200×200 mm^2; matrix =64×64; slice thickness =5.4 mm; slice gap =1.2 mm; flip angle =90, slice orientation: axial, and order of slice accession: interleaved, and duration =8 minutes and 6 seconds. In addition, a sagittal 3D T1-weighted gradient-echo sequence was acquired using the following parameters : 176 structural images, TR =1,900 ms, TE =2.26 ms, slice thickness =1 mm, slice gap =0.5 mm, matrix =56×256, FOV =250×250 mm^2, flip angle =9, and duration =3 minutes and 34 seconds.

Data pre-processing

All rs-fMRI data was subjected to pre-processing using Data Processing Assistant for Resting-State fMRI software (DPARSF 5.0, http://restfmri.net/forum/DPARSF) (27). Pre-processing included removal of the first 10 volumes, slice timing, re-alignment, and spatial normalization to the standard Montreal Neurological Institute (MNI) 152 template with a re-sampling voxel size of 3×3×3 mm^3. Spatial smoothing was then performed with an 8-mm full-width at half-maximum (FWHM) Gaussian kernel. Linear detrending of the BOLD signal and temporal filtering of band-pass (0.01–0.08 Hz) was conducted to remove low-frequency drift and high-frequency physiological noise.

Nuisance signals were then regressed out, including cerebrospinal fluid signals, global mean signals, white matter signals, and Friston-24 head motion parameters. The information of framewise displacement of the resting-state fMRI images in CSM and HC are showed in online: https://cdn.amegroups.cn/static/public/qims-20-874-1.zip.

Functional network construction and analysis

Node definition
A functional network was constructed for each participant using a graph theoretical network analysis (GRETNA) toolbox 2.0.0 (http://www.nitrc.org/projects/gretna) (27,28). Networks were constructed with edges representing connections among nodes, with nodes representing brain regions. Automated anatomical labeling (AAL) atlas was used to divide the brain into 116 anatomical regions (Figure S1), including 78 cortical, 12 subcortical, and 26 cerebellar areas (29). Each region was regarded as a network node.

Edge definition
Time series were extracted by averaging voxel signals within each region to define the network edge. Partial correlation coefficients of each pair of nodes were calculated between the regional average temporal series, correcting for effects of the remaining 114 regions (representing their conditional dependencies). A 116×116 symmetric partial correlation matrix was produced for each included subject, and individual partial correlation matrices were converted into binarized matrices to eliminate weaker connections based on a pre-defined threshold (22).

Threshold selection
There are no available gold-standard criteria to determine a precise sparsity threshold. Therefore, we explored graph correlation matrices with a wide range of sparsity thresholds from 0.1 to 0.34, with an interval of 0.01. This resulted in 25 sparse connectivity matrices, as reported in previous studies (22,30). The minimum and maximum values of the sparsity threshold were established to ensure that thresholded networks were estimable for small-worldness (σ) scalar and that σ was greater than 1.0 (31).

Global and local measures
The topological properties of the functional brain network were calculated at global and nodal levels. Global topological properties included: (I) small-world parameters including Lp, Cp, λ, normalized clustering coefficient (γ), and σ; and (II) network efficiency including global efficiency ($Eglob$) and local efficiency ($Eloc$). Nodal level properties included nodal degree, nodal efficiency, and nodal betweenness. These network properties have previously been defined by Zhang *et al.* (22), and a brief interpretation of these network characteristics is provided in Table S1. The equation and explanation of these were showed in Supplementary File. Moreover, the area under the curve (AUC) of all network metrics was constructed over the whole range of the sparsity threshold. The AUC provides a summarized scalar for the topological characterization of brain networks, independent of a single threshold selection, sensitive in detecting topological alterations of brain disorders, and unravel between-group differences in network organization.

Statistical analysis

Differences in demographic and clinical variables
Statistical analyses were conducted using R software version 4.0.0. The difference in categorical variables between groups was tested and compared using a chi-squared test, while that between continuous variables was evaluated using a two-sample t-test.

Group comparisons based on topological metrics
To evaluate differences of network metrics between CSM and HCs groups, the AUC of each network metric was compared using a nonparametric permutation test, and P values were corrected by the Benjamini-Hochberg false discovery rate (FDR q value <0.05) (32). If between-group significant differences were observed in any network metrics, exploratory partial correlation analysis was conducted to assess the relationships between network parameters; disease duration, the Japanese Orthopedic Association (JOA) score, and Neck Disability Index (NDI) score in the CSM group with age and gender as covariates (P values corrected with FDR q value <0.05) (33,34).

Results

Demographics and clinical characteristics

There was no significant difference in sex (P=0.902), age (P=0.220) and education level (P=0.462) between CSM patients and HCs. CSM patients had a mean symptom

Table 1 Demographic and clinical characteristics of the subjects

Clinical variables	CSM (n=67)	HC (n=60)	P value
Age	47.52±7.36	45.51±10.64	0.220
Gender (male/female)	35/32	32/28	0.902
Education (years)	12.88±1.32	12.53±1.53	0.462
Duration of symptoms (month)	10.86±6.68	NA	–
NDI scores	0.301±0.094	NA	–
JOA scores	10.32±2.53	NA	–
Motor upper	2.33±0.67	NA	–
Motor lower	2.78±1.02	NA	–
Sensory deficit	3.38±0.65	NA	–
Bladder dysfunction	2.17±0.47	NA	–

CSM, cervical spondylotic myelopathy; HC, healthy control; NDI, Neck Disability Index; JOA, Japanese Orthopedic Association.

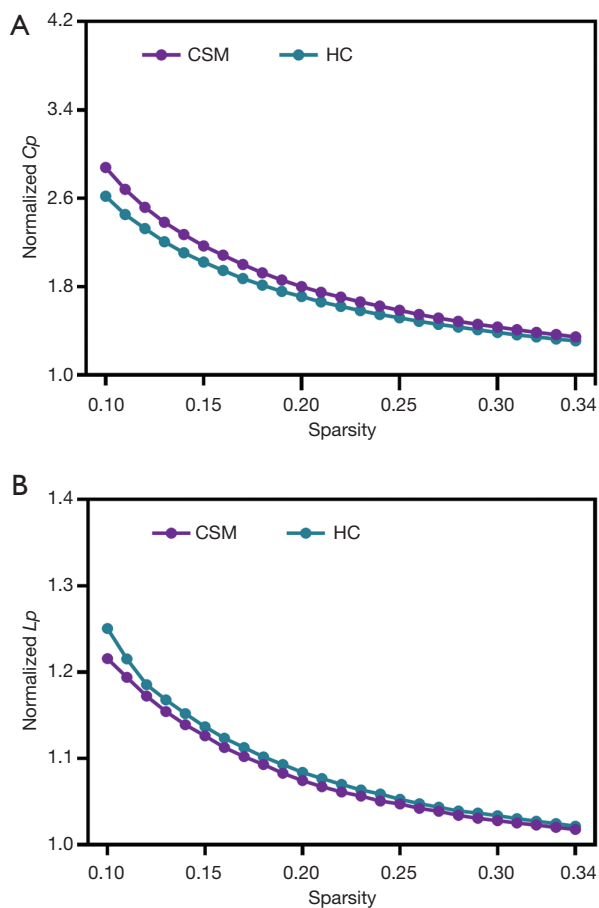**Figure 1** Small-world properties in functional brain networks demonstrated in CSM patients in the range of sparsity thresholds (0.1< S <0.34), with (A) normalized clustering coefficient (Cp) (γ) >1 and (B) normalized characteristic path length (Lp) (λ) ≈1.

duration of 10.86±6.68 months, mean JOA score of 10.32±2.53, and mean NDI score of 0.301±0.094 (*Table 1*).

CSM-related alterations in small-world properties

Small-world properties were recorded in both CSM patients and HCs across the whole range of cost thresholds (0.1–0.34), with γ >1 and λ ≈1 (*Figure 1*). Compared with HCs, CSM patients had a significantly lower characteristic path length (Lp) (FDR q=0.040), clustering coefficient Cp (FDR q=0.037), and λ (FDR q=0.038), and a significantly higher normalized γ (FDR q=0.014) and σ (FDR q=0.009). While CSM patients exhibited significantly higher global efficiency $Eglob$ (FDR q=0.027), there was no significant difference in local efficiency $Eloc$ (FDR q=0.440) between CSM patients and HCs (*Figure 2*).

CSM-related alterations in regional nodal characteristics

Brain regions showing significant between-group differences in at least one nodal metric (P<0.05, FDR corrected) were identified. Compared to HCs, CSM patients exhibited higher nodal centralities in the bilateral inferior cerebellum, medial orbital part of right superior frontal gyrus (ORBsupmed), left anterior cingulate and paracingulate gyri (ACG), left median cingulate gyrus (DCG), bilateral precuneus, bilateral angular gyrus, and medial part of the bilateral superior frontal gyrus (SFGmed). In contrast, compared to the HCs group, CSM patients exhibited lower nodal centralities in the bilateral
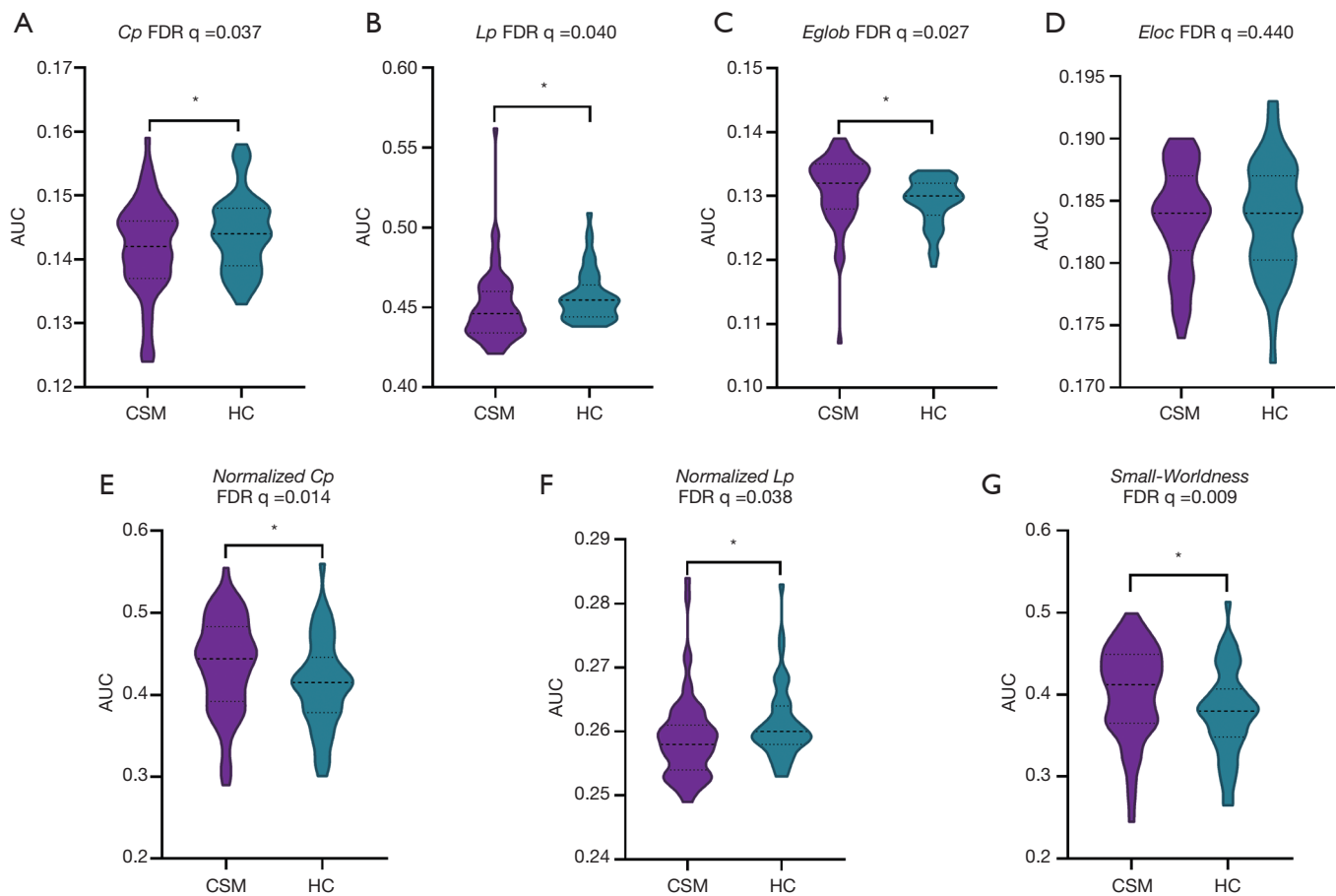
Figure 2 Between-group comparisons of; (A) clustering coefficient (*Cp*), (B) characteristic path length (*Lp*), (C) global efficiency (*Eglob*), (D) local efficiency (*Eloc*), (E) normalized clustering coefficient (γ), (F) normalized characteristic path length (λ), and (G) small-worldness (σ). *FDR q<0.05.

lingual gyrus, bilateral posterior cingulate gyrus (PCG), bilateral putamen, left postcentral gyrus (PoCG), and right middle temporal gyrus (MTG) (*Table 2* and *Figure 3*).

Relationships between network measures and clinical variables

The Japanese Orthopedic Association (JOA) score was positively correlated with global efficiency (r =0.3825, FDR q=0.0014) and negatively correlated with characteristic path length (r =−0.429, FDR q=0.0003). Nodal degree in the left PoCG (r =0.366, FDR q=0.02) and nodal efficiency in the left putamen (r =0.363, FDR q=0.02) were positively correlated with JOA score (*Figure 4*), and there was no correlation between disease duration, NDI score, and global or nodal network parameters.

Discussion

The present study used resting-state fMRI to explore changes in the topological organization of functional brain networks in CSM patients and, to the best of our knowledge, is the first study to investigate the "small-world" brain functional network in CSM patients. Both CSM patients and HCs exhibited small-world properties of functional brain networks, characterized by high local clustering and short path length. However, despite having similar small-world topology, CSM patients exhibited significantly low *Cp*, *Lp*, and normalized λ and high γ, σ, and *Eglob*. In local brain regions, nodal topological properties revealed group differences predominantly in the default-mode network, visual cortex, and sensory-motor regions. In particular, CSM patients recorded low nodal centralities in the bilateral lingual gyrus, bilateral

3424

Cao et al. Graph theory analysis of CSM

Table 2 Regions showing abnormal nodal centralities in CSM patients as compared with healthy controls

Brain regions	FDR q values		
	Nodal degree	Nodal efficiency	Nodal betweenness
CSM patients > healthy control subjects			
Left inferior cerebellum	**0.0128**	**0.0085**	**0.0437**
Right inferior cerebellum	**0.0467**	**0.0235**	**0.0146**
Right superior frontal gyrus, medial orbital	**0.0076**	**0.0052**	**0.0398**
Left superior frontal gyrus, medial	**0.0094**	**0.0059**	0.3539
Right superior frontal gyrus, medial	**0.0022**	**0.0012**	0.2947
Left anterior cingulate and paracingulate gyri	0.3350	0.3803	**0.0476**
Left median cingulate gyrus	0.2392	0.2196	**0.0441**
Left precuneus	**0.0040**	**0.0022**	0.3437
Right precuneus	**0.0004**	**0.0002**	0.2598
Left angular gyrus	0.0850	**0.0491**	0.2673
Right angular gyrus	**0.0424**	**0.0351**	0.1028
CSM patients < healthy control subjects			
Left postcentral gyrus	0.2837	0.1715	**0.0346**
Left putamen	**0.0037**	**0.0147**	0.1483
Right putamen	**0.0251**	**0.0365**	0.4156
Left lingual gyrus	0.0984	0.1071	**0.0329**
Right lingual gyrus	**0.0309**	**0.0442**	**0.0351**
Left posterior cingulate gyrus	**0.0035**	**0.0015**	0.3823
Right posterior cingulate gyrus	**0.0057**	**0.0023**	0.4109
Right middle temporal gyrus	0.2841	0.4540	**0.0026**

Regions were considered abnormal in CSM patients if they exhibited significant between-group differences (FDR q<0.05) in at least one of the three nodal centralities (shown in bold font). CSM-cervical spondylotic myelopathy.

PCG, bilateral putamen, left PoCG, and right MTG, while in contrast, they exhibited high nodal centralities in the bilateral inferior cerebellum, right ORBsupmed, left ACG, left DCG, bilateral precuneus, bilateral angular gyrus, and bilateral SFGmed. These results indicated a disturbance of the normal local specialization and global integration and segregation of whole-brain networks in CSM patients and may partly reflect the clinical symptoms of sensory-motor dysfunction. Also, the results showed topological properties in CSM patients are different from those seen in SCI patients, which may indicate the different mechanisms of injury between the two diseases.

According to the current theory, the brain network is classified into a regular network, a random network, and a "small-world" network, with the regular network having a higher Cp and a longer Lp and random network exhibiting a lower Cp and shorter Lp. Generally, the human brain functional network has a small-world architecture computed with the balance between brain functional segregation and integration, characterized by high Cp and short Lp (18).

Both CSM patients and HCs recorded a $\lambda \approx 1$ and a $\gamma > 1$, pointing to "small-world" brain networks in both groups. However, the study revealed some significant alterations in the global properties, particularly in small-world metrics and network efficiency. Compared with HCs, CSM patients showed a lower Cp, Lp, λ, and higher γ, $Eglob$, and σ, which imply a disturbance of the normal local specialization and global integration of whole-brain networks. The lower Lp,
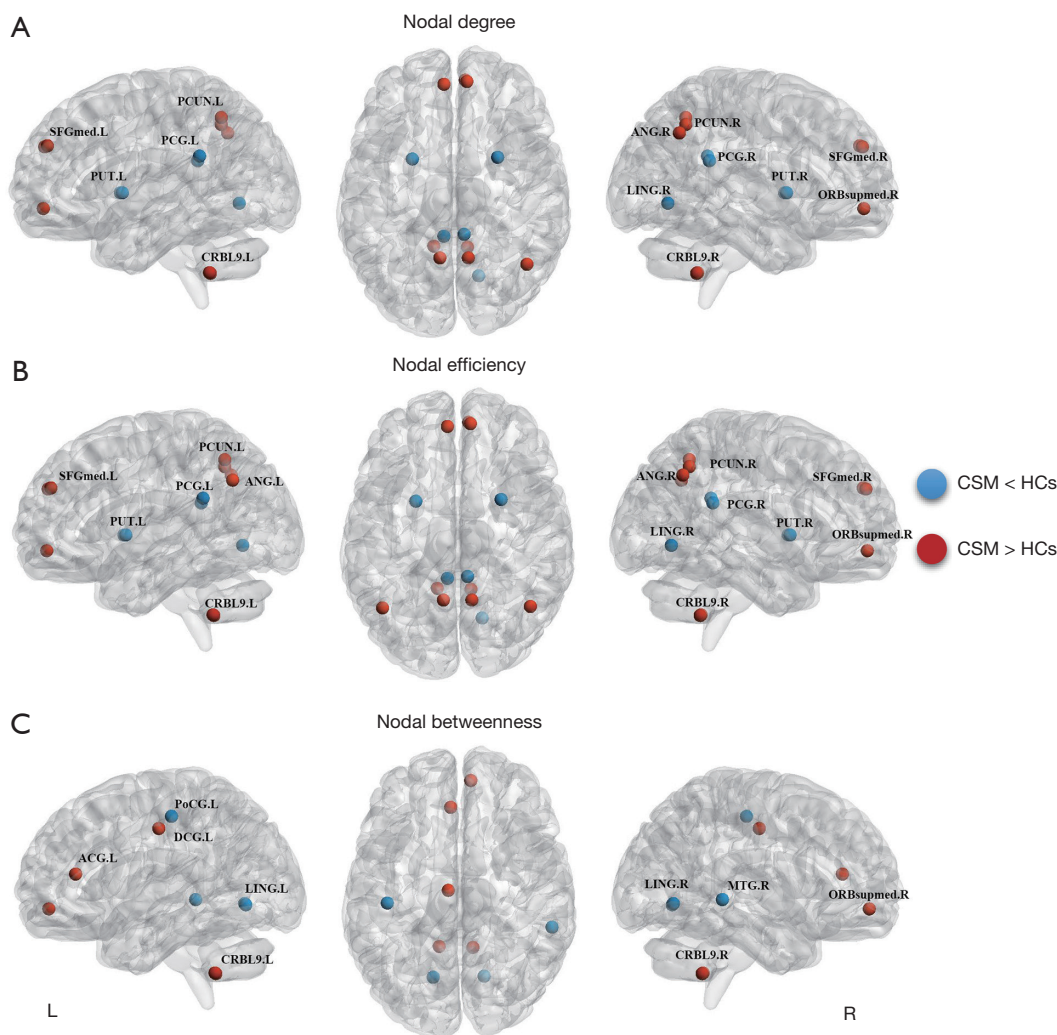
Figure 3 Between-group comparisons of regional nodal characteristics. Red and blue circles represent higher and lower nodal centralities, respectively, as observed in CSM patients compared with healthy controls. CRBL9, bilateral inferior cerebellum; ORBsupmed, superior frontal gyrus, medial orbital; ACG, anterior cingulate and paracingulate gyri; DCG, median cingulate gyrus; PCUN, precuneus; ANG, angular gyrus; SFGmed, superior frontal gyrus, medial; LING, lingual gyrus; PCG, posterior cingulate gyrus; PUT, putamen; PoCG, postcentral gyrus; MTG, right middle temporal gyrus; R, right; L, left.

λ, and *Cp*, and higher *Eglob* indicated a decrease in local specialization and increased global integration in CSM patients. This suggests a shift towards a randomized network in functional brain networks, which is consistent with the results of a recent study focusing on topological properties alteration of brain structural covariance networks in CSM patients (25). This randomization in networks has also been reported in AD, social anxiety disorder (SAD), and MDD (22,35). Zhang *et al.* indicated a shift toward randomization with a lower path length and higher global efficiency in

first-episode MDD patients' brain networks (22). A study focusing on drug-naïve SAD reported a lower λ compared with HC, which also suggested a shift of network topology towards randomized configurations that existed in SAD patients (36). Compared with a small-world network, a random network decomposes into lower modularity of information processing and tolerance of faults (37). Randomization in CSM patients reflects a low optimal topological organization of functional brain networks and is evidence that CSM is not a disease with single damage
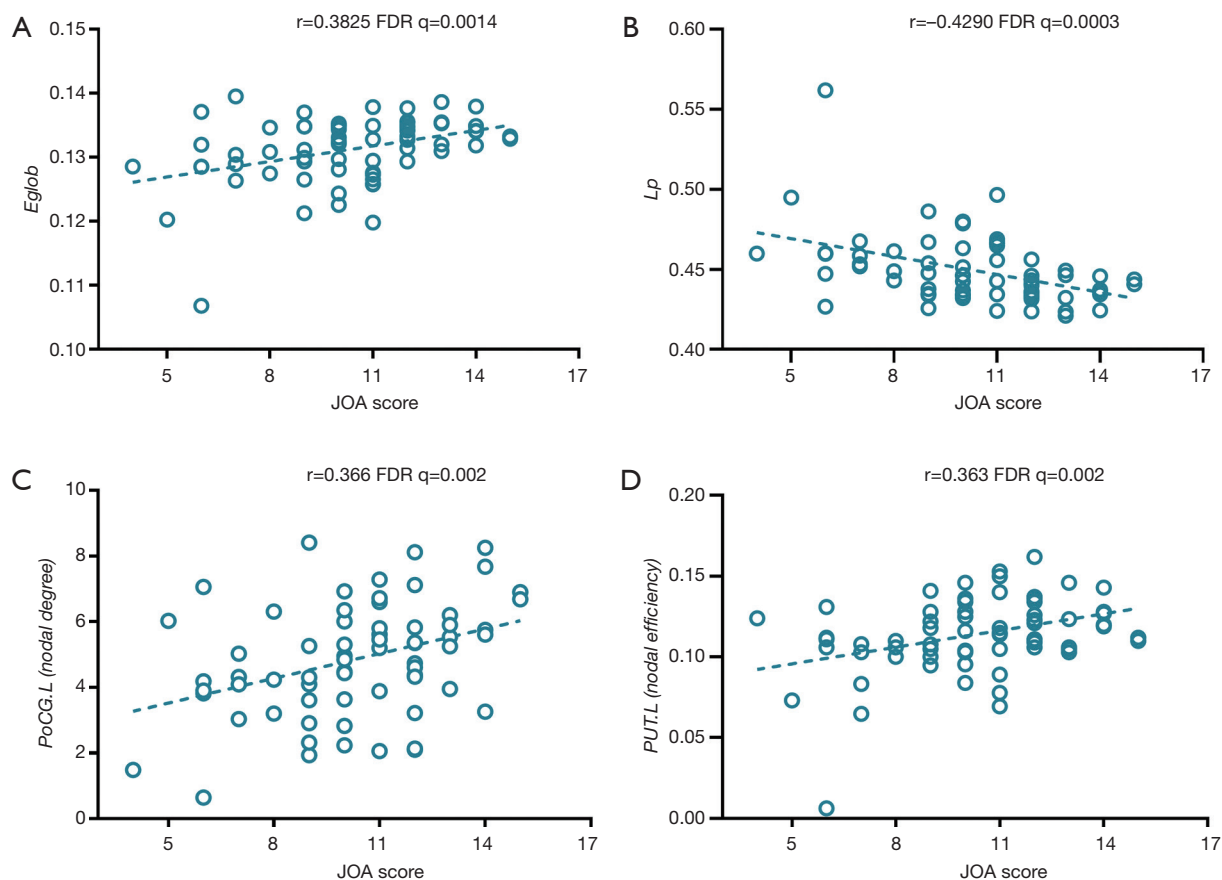
Figure 4 Partial correlation analysis of network measures and clinical variables in CSM patients. The JOA score (A) positive correlation with global efficiency (*Eglob*) and (B) negative correlation with characteristic path length (*Lp*). JOA score positive correlation with (C) nodal degree in the left postcentral gyrus (PoCG.L) and (D) nodal efficiency in the left putamen (PUT.L)

to cervical cord injury but one with disrupted neuronal network organization. This disruption may shed light on the clinical symptoms of neck pain comorbid with anxiety and depression in CSM patients, although the current study did not evaluate the level of anxiety or depression, and further research should value these to reduce the risk of bias. Notably, this study revealed that the JOA score is positively correlated with *Eglob* and negatively correlated with *Lp* in CSM patients, which implies that the higher the severity of sensory-motor dysfunction in CSM, the lower the integration capability of brain functional networks. Notably, we found an increased σ in CSM patients compared with HC and that the σ would decrease in the patient group in which impaired function was presented. This contrasts with the results of Wen *et al.* who found an increased σ in Tourette syndrome patients compared with HC but did not speculate on a reason for this. We speculate

that this seemingly conflictive result might be due to compensatory mechanisms in CSM patients.

Abnormal nodal centralities were mainly located in the sensory-motor region, visual cortex, and DMN, and the results showed reduced nodal centralities in the left PoCG, bilateral putamen, bilateral lingual gyrus, and bilateral PCG. The PoCG is a prominent gyrus in the primary somatosensory cortex and has been shown to play a vital role in hand movement (38). Reduced nodal centrality in this area is related to sensory impairment in CSM patients, corresponding to numbness, and a positive correlation was observed between the nodal degree of left PoCG and the JOA score. The putamen is dedicated primarily to motor control and decreased nodal betweenness. It implies severely and progressively hindered motor function. Nodal efficiency in the left putamen was positively correlated with the JOA score, indicating a close relationship between the

left putamen's nodal centralities and the impaired motor function. The lingual gyrus is the vision center in the human brain and has been shown to play a role in visual processing and perception of emotions (39,40). Decreased ALFF and ReHo values in the primary visual cortex have been reported to be related to blurred vision in CSM patients (15), and this is consistent with our findings of decreased nodal centrality in the bilateral lingual gyrus. The DMN is known as the task-negative network (41), which has been reported to be involved in the processing of self-referential, introspective state, and spontaneous cognition, and mediates human feelings and thoughts DMN disruption has been observed in the spinal cord injury and CSM patients. In an animal study, PCG, as a component of DMN, has been shown to have a direct relationship with motor function (42). Decreased PCG activity recorded after spinal cord injury is consistent with the findings of this study. While our results showed increased nodal centralities in the DMN including SFGmed, ORBsupmed, ACG, DCG, bilateral precuneus, bilateral angular gyrus, and right MTG, which may indicate an inhabitation of sensory-motor function, whether these brain areas are related to brain reorganization of CSM should further be verified in longitudinal studies. Also, whether increased nodal centralities in the DMN implies an increase in psychological processing activity requires further studied. Increased nodal centralities were recorded in the bilateral inferior cerebellum. The cerebellum is involved in sensory-motor integration, motor coordination, and sensory acquisition and the increased nodal centralities here may indicate a compensation to motor-sensory dysfunction in CSM patients (43). Our results are also partly consistent with previous studies by Kuang *et al.* (25), although they found greater nodal betweenness in the left superior parietal gyrus and the left supplementary motor area when compared with controls.

Limitations

There are several limitations to the current study that warrant consideration. First, although this cross-sectional study identified large-scale brain network alterations intrinsic to CSM, longitudinal studies are needed to determine the effect of decompression surgery on these alterations and would provide further evidence on brain remodeling mechanisms. Secondly, only 116 AAL templates were used in constructing brain functional networks. Although this has been considered adequate in several

studies, employing more brain templates could produce a different outcome. Thirdly, to minimize the effect of age-related brain deterioration, only patients aged between 18 and 65 years were included, although it has been reported that the incidence of CSM significantly increases after the age of 60 years. Fourthly, although we found that global and regional topological quantifications were different between CSM patients and normal populations, the global topological properties of shifting toward randomization were also found in MDD. This may indicate functional MRI-based topological graph analysis only detects general global brain functional changes common to central nervous system diseases and may not have specificity to detect or distinguish individual disease. Fifth, the CSM patients in the current study did not undergo comprehensive cognitive scales testing, which could have prevented a more accurate detection of cognitive performance and an analysis of the correlation between cognitive performance and small-world properties. Moreover, although graph theory-based brain networks can elucidate complicated spatiotemporal patterns for functional organization and are applied on a macroscopic level to help us better understand the working mechanism of small-world human brain networks, the neurobiological basis that underlies brain disorders, as well as provide a potential neuroimage biomarker that is specific to a disease or clinical symptoms, more research is required before this can be applied in clinical practice. Finally, the current study did not record the severity of spinal cord compression including the ellipticity of the compressed spinal cord or the existence of myelomalacia, and studies which analyze the relationship between the severity of the spinal cord compression and randomness of the global brain network are also required.

Conclusions

This study investigated alterations in the topological organization of functional brain networks in CSM patients. Compared with HCs, CSM patients exhibited lower characteristic path length, normalized characteristic path length and clustering coefficient, higher normalized clustering coefficient, small-worldness, and global efficiency. Several local brain regions were profoundly affected by CSM including decreased nodal centralities in the left PoCG, bilateral putamen, lingual gyrus, and PCG, which is indicative of sensory-motor and visual dysfunction. Increased nodal centralities in the cerebellum may be a basis

3428

Cao et al. Graph theory analysis of CSM

for compensatory in sensory-motor dysfunction in CSM patients, although whether the increased nodal centralities in DMN is related to the processing of self-referential requires further verification.

Footnote

Conflicts of Interest: All authors have completed the ICMJE uniform disclosure form (available at http://dx.doi.org/10.21037/qims-20-874). The authors have no conflicts of interest to declare.

Ethical Statement: The authors are accountable for all aspects of the work in ensuring that questions related to the accuracy or integrity of any part of the work are appropriately investigated and resolved. This study was approved by the Institutional Review Board of the First Affiliated Hospital of Nanchang University and was conducted following ethical principles for medical research involving human subjects as stipulated in the World Medical Association's Declaration of Helsinki (as revised in 2013). Written informed consent was obtained from each subject prior to the study.

References

1. Lees F, Turner JW. Natural history and prognosis of cervical spondylosis. Br Med J 1963;2:1607-10.
2. Nouri A, Tetreault L, Singh A, Karadimas SK, Fehlings MG. Degenerative Cervical Myelopathy: Epidemiology, Genetics, and Pathogenesis. Spine (Phila Pa 1976) 2015;40:E675-93.
3. Zhuang L, Wang L, Xu D, Wang Z, Liang R. Association between excessive smartphone use and cervical disc degeneration in young patients suffering from chronic neck pain. J Orthop Sci 2021;26:110-5.
4. Engstrom J. Cervical spondylotic myelopathy. 2017.
5. Karpova A, Arun R, Davis AM, Kulkarni AV, Massicotte EM, Mikulis DJ, Lubina ZI, Fehlings MG. Predictors of surgical outcome in cervical spondylotic myelopathy. Spine (Phila Pa 1976) 2013;38:392-400.
6. Lee JJ, Lee N, Oh SH, Shin DA, Yi S, Kim KN, Yoon DH, Shin HC, Ha Y. Clinical and radiological outcomes of multilevel cervical laminoplasty versus three-level anterior cervical discectomy and fusion in patients with cervical spondylotic myelopathy. Quant Imaging Med Surg 2020;10:2112-24.
7. Holly LT. Management of cervical spondylotic myelopathy with insights from metabolic imaging of the spinal cord and brain. Curr Opin Neurol 2009;22:575-81.
8. Holly LT, Dong Y, Albistegui-DuBois R, Marehbian J, Dobkin B. Cortical reorganization in patients with cervical spondylotic myelopathy. J Neurosurg Spine 2007;6:544-51.
9. Raineteau O, Schwab ME. Plasticity of motor systems after incomplete spinal cord injury. Nat Rev Neurosci 2001;2:263-73.
10. Sabbah P, de SS, Leveque C, Gay S, Pfefer F, Nioche C, Sarrazin JL, Barouti H, Tadie M, Cordoliani YS. Sensorimotor cortical activity in patients with complete spinal cord injury: a functional magnetic resonance imaging study. J Neurotrauma 2002;19:53-60.
11. Duggal N, Rabin D, Bartha R, Barry R, Gati J, Kowalczyk I, Fink M. Brain reorganization in patients with spinal cord compression evaluated using fMRI. Neurology 2010;74:1048-54.
12. Zhou FQ, Tan YM, Wu L, Zhuang Y, He LC, Gong HH. Intrinsic functional plasticity of the sensory-motor network in patients with cervical spondylotic myelopathy. Sci Rep 2015;5:9975.
13. Zhou F, Gong H, Liu X, Wu L, Luk KD, Hu Y. Increased low-frequency oscillation amplitude of sensorimotor cortex associated with the severity of structural impairment in cervical myelopathy. PLoS One 2014;9:e104442.
14. Tan Y, Zhou F, Wu L, Liu Z, Zeng X, Gong H, He L. Alteration of Regional Homogeneity within the Sensorimotor Network after Spinal Cord Decompression in Cervical Spondylotic Myelopathy: A Resting-State fMRI Study. Biomed Res Int 2015;2015:647958.
15. Chen Z, Wang Q, Liang M, Zhao R, Zhu J, Xiong W, Su

Z, Yu C, Xue Y. Visual cortex neural activity alteration in cervical spondylotic myelopathy patients: a resting-state fMRI study. Neuroradiology 2018;60:921-32.

16. Kuang C, Zha Y. Abnormal intrinsic functional activity in patients with cervical spondylotic myelopathy: a resting-state fMRI study. Neuropsychiatr Dis Treat 2019;15:2371.

17. Bullmore E, Sporns O. Complex brain networks: graph theoretical analysis of structural and functional systems. Nat Rev Neurosci 2009;10:186-98.

18. Watts DJ, Strogatz SH. Collective dynamics of 'small-world' networks. Nature 1998;393:440-2.

19. Min YS, Chang Y, Park JW, Lee JM, Cha J, Yang JJ, Kim CH, Hwang JM, Yoo JN, Jung TD. Change of Brain Functional Connectivity in Patients With Spinal Cord Injury: Graph Theory Based Approach. Ann Rehabil Med 2015;39:374-83.

20. Ponten S, Bartolomei F, Stam C. Small-world networks and epilepsy: graph theoretical analysis of intracerebrally recorded mesial temporal lobe seizures. Clin Neurophysiol 2007;118:918-27.

21. He Y, Chen Z, Evans A. Structural insights into aberrant topological patterns of large-scale cortical networks in Alzheimer's disease. J Neurosci 2008;28:4756-66.

22. Zhang J, Wang J, Wu Q, Kuang W, Huang X, He Y, Gong Q. Disrupted brain connectivity networks in drug-naive, first-episode major depressive disorder. Biol Psychiatry 2011;70:334-42.

23. Chen L, Li S, Cai F, Wu L, Gong H, Pei C, Zhou F, Zeng X. Altered functional connectivity density in primary angle-closure glaucoma patients at resting-state. Quant Imaging Med Surg 2019;9:603-14.

24. Peng X, Tan Y, He L, Ou Y. Alterations of functional connectivity between thalamus and cortex before and after decompression in cervical spondylotic myelopathy patients: a resting-state functional MRI study. Neuroreport 2020;31:365-71.

25. Kuang C, Zha Y, Liu C, Chen J. Altered Topological Properties of Brain Structural Covariance Networks in Patients With Cervical Spondylotic Myelopathy. Front Hum Neurosci 2020;14:364.

26. Hojjati SH, Ebrahimzadeh A, Babajani-Feremi A. Identification of the Early Stage of Alzheimer's Disease Using Structural MRI and Resting-State fMRI. Front Neurol 2019;10:904-.

27. Yan C, Zang Y. DPARSF: a MATLAB toolbox for" pipeline" data analysis of resting-state fMRI. Front Syst Neurosci 2010;4:13.

28. Wang J, Wang X, Xia M, Liao X, Evans A, He Y.

GRETNA: a graph theoretical network analysis toolbox for imaging connectomics. Front Hum Neurosci 2015;9:386.

29. Tzourio-Mazoyer N, Landeau B, Papathanassiou D, Crivello F, Etard O, Delcroix N, Mazoyer B, Joliot M. Automated anatomical labeling of activations in SPM using a macroscopic anatomical parcellation of the MNI MRI single-subject brain. Neuroimage 2002;15:273-89.

30. Chen Y, Huang X, Wu M, Li K, Hu X, Jiang P, Chen L, He N, Dai J, Wang S. Disrupted brain functional networks in drug-naïve children with attention deficit hyperactivity disorder assessed using graph theory analysis. Hum Brain Mapp 2019;40:4877-87.

31. Humphries MD, Gurney K, Prescott TJ. The brainstem reticular formation is a small-world, not scale-free, network. Proc Biol Sci 2006;273:503-11.

32. Genovese CR, Lazar NA, Nichols T. Thresholding of statistical maps in functional neuroimaging using the false discovery rate. Neuroimage 2002;15:870-8.

33. Vernon H. The Neck Disability Index: state-of-the-art, 1991-2008. J Manipulative Physiol Ther 2008;31:491-502.

34. Azimi P, Mohammadi HR, Montazeri A. An outcome measure of functionality and pain in patients with lumbar disc herniation: a validation study of the Japanese Orthopedic Association (JOA) score. J Orthop Sci 2012;17:341-5.

35. Sanz-Arigita EJ, Schoonheim MM, Damoiseaux JS, Rombouts SA, Maris E, Barkhof F, Scheltens P, Stam CJ. Loss of 'small-world' networks in Alzheimer's disease: graph analysis of FMRI resting-state functional connectivity. PLoS One 2010;5:e13788.

36. Yang X, Liu J, Meng Y, Xia M, Cui Z, Wu X, Hu X, Zhang W, Gong G, Gong Q. Network analysis reveals disrupted functional brain circuitry in drug-naive social anxiety disorder. Neuroimage 2019;190:213-23.

37. Latora V, Marchiori M. Efficient behavior of small-world networks. Phys Rev Lett 2001;87:198701.

38. Li Y, Zhang S, Jin Y, Cai B, Controzzi M, Zhu J, Zhang J, Zheng X. Gesture decoding using ECoG signals from human sensorimotor cortex: A pilot study. Behav Neurol 2017;2017:3435686.

39. Zhang L, Wang H, Luan S, Yang S, Wang Z, Wang J, Zhao H. Altered volume and functional connectivity of the Habenula in Schizophrenia. Front Hum Neurosci 2017;11:636.

40. Tao H, Guo S, Ge T, Kendrick KM, Xue Z, Liu Z, Feng J. Depression uncouples brain hate circuit. Mol Psychiatry 2013;18:101-11.

3430

Cao et al. Graph theory analysis of CSM

41. Raichle ME, MacLeod AM, Snyder AZ, Powers WJ, Gusnard DA, Shulman GL. A default mode of brain function. Proc Natl Acad Sci U S A 2001;98:676-82.

42. Rao JS, Ma M, Zhao C, Liu Z, Yang ZY, Li XG. Alteration of brain regional homogeneity of monkeys with spinal cord injury: a longitudinal resting-state functional magnetic resonance imaging study. Magn Reson Imaging 2015;33:1156-62.

43. Ohyama T, Nores WL, Murphy M, Mauk MD. What the cerebellum computes. Trends Neurosci 2003;26:222-7.

Equation and explanation

1. $Cp = \sum_{i \in N} \dfrac{2ti}{ki(ki-1)}$

The clustering coefficient was regarded as the probability of finding a connection between any two neighbors of node i, k_i is the degree of node i, and t_i is the number of closed triangles attached to i (44).

2. $Lp = \dfrac{1}{N} \sum_{i} li = \dfrac{1}{N(N-1)} \sum_{i \neq j} lij$

l_i is the average shortest path length from node i to all other nodes and l_{ij} is the shortest path length from node j to node i, which is computed with Dijkstra's algorithm or one of its variants. This formulation is applicable to both directed and undirected networks (44).

3. $\gamma = \dfrac{Cp}{Cprand}$

Cp_{rand} is the average clustering coefficient computed in an ensemble of randomized surrogate networks (44).

4. $\lambda = \dfrac{Lp}{Lprand}$

Lp is the average shortest path length between nodes in the network. Lp_{rand} is the average shortest path length computed in an ensemble of randomized surrogate networks (44).

5. $\sigma = \dfrac{\gamma}{\lambda}$

This index is a ratio of the normalized clustering and path length measures (44).

6. $Eglob = \dfrac{1}{N(N-1)} \sum_{i \neq j} \dfrac{1}{lij}$

E_{glob} is the reciprocal of the harmonic mean of its path lengths (44).
G_i denotes the subgraph comprising all nodes that are immediate neighbors of the ith node (44).

7. $Eloc = \dfrac{1}{NGi(NGi-1)} \sum_{j,h \in Gi} \dfrac{1}{jh'}$

References

44. Fornito A, Zalesky A, Bullmore E. Fundamentals of brain network analysis: Academic Press; 2016.
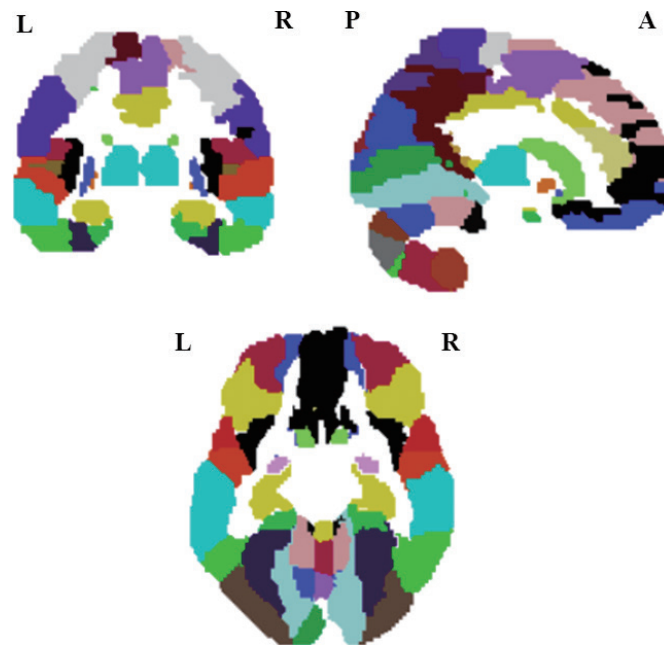
Figure S1 Automated anatomical labeling (AAL) atlas. Different colors represent different regions. L = left; R = right; P=Posterior; A = anterior.

Table S1 Brief introduction of network metrics

Network metrics	Definition
Clustering coefficient (Cp)	A measure of network average local density
Characteristic path length (Lp)	The average of the shortest path lengths between any pair of nodes in the network.
Normalized Cp (γ)	The ratio of the Cp between real and random networks
Normalized Lp (λ)	The ratio of the Lp between real and random networks
Small-worldness (σ)	Scalar quantitative measurement of the small-wordness of a network
Global efficiency ($Eglob$)	A measure of the global efficiency of parallel information transfer in the network
Local efficiency ($Eloc$)	A measure of the fault tolerance of the network